ISSN 0023-1584, Kinetics and Catalysis, 2009, Vol. 50, No. 1, pp. 122–130. © Pleiades Publishing, Ltd., 2009.
Original Russian Text © V.Yu. Gavrilov, O.P. Krivoruchko, 2009, published in Kinetika i Kataliz, 2009, Vol. 50, No. 1, pp. 132–140.

Synthesis and Mesopore–Micropore Structure Characterization of Nanodisperse Fe^{3+} Hydrogels (Xerogels)

V. Yu. Gavrilov and O. P. Krivoruchko

Boreskov Institute of Catalysis, Siberian Branch, Russian Academy of Sciences, Novosibirsk, 630090 Russia
e-mail: gavrilov@catalysis.ru

Received July 16, 2007

Abstract—A preparation procedure was developed, and samples of nanodisperse Fe^{3+} hydroxide with a narrow particle-size distribution (2.5–3.5 nm) were synthesized. The occurrence of a substructure in the bulk of Fe^{3+} hydroxide nanoparticles was detected for the first time using light-field and dark-field transmission electron microscopy. It was found that structurally ordered regions with sizes of ~1.0 nm, which were disoriented with respect to each other at angles of a few degrees, occurred in the bulk of the nanoparticles. The empirical formula of nanodisperse iron hydroxide was $\sim Fe_2O_3 \cdot 1.8H_2O$; the structure of this hydroxide contained crystal water, OH^-, and O^{2-}. The coordination number of Fe^{3+} cations with respect to oxygen was 6. It was found that both structural and nonstructural water can be removed almost completely from the bulk of nanoparticles in the course of sample heating to 150–250°C in a vacuum with the retention of their amorphous character and observed sizes. In the course of dehydration, the mutual mobility of nanoparticles within aggregates was retained in Fe^{3+} xerogels; this resulted in a decrease in the total pore volume, whereas the volume of mesopores with diameters of 3.4–3.5 nm progressively increased. The micropore structure of the samples of nanodisperse iron hydroxides was studied by the molecular probe method using the low-temperature (77 K) sorption of nitrogen and molecular hydrogen. It was found that, along with micropores of volume ~0.02 cm^3/g, which are accessible to both of the sorbates, the sorption of H_2 exhibited an additional specific absorption of 1.0–1.7 cm^3(STP)/g, which can be interpreted as an additional ultramicropore volume accessible to only hydrogen molecules.

DOI: 10.1134/S0023158409010169

INTRODUCTION

Iron oxides are commonly used as catalyst precursors [1–5] and catalysts [6–11]. Catalysts containing promoted iron oxides are used in the commercial dehydrogenation of alkylaromatic and olefin hydrocarbons to obtain monomers for synthetic rubbers [1–3]. Superacid catalysts based on sulfated iron oxides [4] and gold on iron hydroxide catalysts for the low-temperature oxidation of CO to CO_2 [5] are well known. A highly efficient catalyst based on nanodisperse Fe^{3+} hydroxides was developed for the low-temperature conversion of ortho-H_2 into para-H_2 [6, 7]. A catalyst known under the trade name NANOCAT® is in wide use abroad; it has been successfully used in mixed rocket fuel to increase the rate of combustion [8] and in the processes of high-temperature CO oxidation [9], direct catalytic coal liquefaction [10, 11], etc.

There are indications that the high efficiency of iron-containing catalysts is due to their nanodisperse state and favorable phase composition (Fe^{3+} oxide hydroxide). Thus, at a reaction temperature of 350°C, the degrees of CO conversion into CO_2 on a NANOCAT® catalyst (particle size of 3 nm) and a coarsely dispersed α-Fe_2O_3 oxide were 100 and 5%, respectively [9]. Daniells et al. [5] found that a 100% degree of CO oxidation at room temperature was reached on a catalyst with 3.4 wt % Au supported on nanodisperse Fe^{3+} hydroxide (ferrihydrite); this catalyst was stable for tens of hours. At the same time, a catalyst of the same composition but prepared with the use of a coarsely dispersed α-Fe_2O_3 oxide exhibited much lower selectivity and stability in this process. Of course, the activity and selectivity of iron oxide catalysts depend not only on the particle size, but also on the pore structure.

The mechanism of formation of insoluble Fe^{3+} hydroxides has been determined previously [12–14]. It was found that polynuclear hydroxo complexes are formed in the interaction of Fe^{3+} aqua cations with a base in aqueous solutions. So-called key polynuclear hydroxo complexes, which are building blocks for the formation of nanosized iron hydroxide particles, are formed in a series of mutual transformations of Fe^{3+} hydroxo complexes. The key polynuclear hydroxo complexes consist of double chains of the oxygen octahedrons $Fe^{3+}(H_2O, OH^-, O^{2-})_6$. Adjacent octahedra are edge-shared through OH^- and O^{2-} bridging groups. In the OH^- bridging groups, which join two adjacent Fe^{3+} cations, electron density is transferred from the O–H bond to the cations; because of this, hydrogen atoms become Brønsted acid sites. Moreover, OH^- groups, which exhibit basic properties, can enter into the coor-

Table 1. Texture characteristics of the nano-GZh-1 samples

Sample no.	Thermal treatment conditions, °C/time, h	γ	S_{BET}, m^2/g	C_{BET}	$S_\alpha^{N_2}$, m^2/g	$V_\mu^{H_2}$, cm^3/g	V_s, cm^3/g	S_{out}, m^2/g
1	Air 110/16 + vacuum 100/5	0.022	281	62	326	0.018	0.179	0.7
2	Air 150/16 + vacuum 150/5	0.051	229	55	276	0.014	0.175	0.6
3	Vacuum 150/6	0.105	310	90	315	0.026	0.172	0.4
4	Air 150/16 + vacuum 150/24	0.056	231	56	276	0.015	0.177	0.7
5	Vacuum 150/24	0.114	306	85	318	0.025	0.170	0.7
6	Vacuum 200/5	0.150	267	65	312	0.022	0.168	1.1
7	Vacuum 250/5	0.164	252	58	298	0.019	0.165	0.6

dination sphere of Fe^{3+} cations in the polynuclear hydroxo complex structure. According to estimations [12–14], the size of key polynuclear hydroxo complexes is smaller than the particle size of nanodisperse Fe^{3+} hydroxides formed from these complexes. Therefore, these latter should have a substructure. Consequently, the formation of additional porosity would be expected in the dehydration of hydroxides in the bulk of the resulting Fe^{3+} xerogel particles.

As a rule, the precipitates of insoluble amorphous Fe^{3+} hydroxides are synthesized under nonequilibrium conditions to result in the formation of nanodisperse particles with sizes of about 4 nm. Immediately after the completion of formation reactions, a number of complex physicochemical processes, which are referred to as aging, occur spontaneously in the precipitates in contact with the mother liquor. The most important of these processes is the crystallization of Fe^{3+} hydroxides, which results in considerable changes in their chemical and phase compositions and the size and morphology of crystallized hydroxide particles [15–17]. Because of this, it is difficult to reproducibly prepare nanodisperse iron hydroxide samples and to characterize their properties and texture characteristics in the pure state.

This study was devoted to the development of a procedure for the preparation of nanodisperse iron hydroxides (this procedure allowed us to obtain samples with a narrow nanoparticle size distribution and to prevent their subsequent aging) and the detailed characterization of the mesopore and micropore structure of Fe^{3+} hydrogels (xerogels).

EXPERIMENTAL

Sample preparation. The samples were prepared in accordance with a procedure developed for the synthesis of nanodisperse Fe^{3+} hydroxide with the use of hydrolytic polycondensation of aqua cations. For this purpose, an aqueous ammonia solution with a concentration of 12.5 wt % was added to 3 N aqueous iron nitrate solutions to reach a final value of pH 7.5, at which processes occurred under quasi-equilibrium conditions. Then, a half of the volume of nanodisperse iron hydroxide gel was washed by decantation with distilled water to remove impurity salts (the representative sample was designated as nano-GZh-1) until the appearance of the first signs of precipitate peptization. The second portion of the gel was initially washed with water to remove impurities; then, water in the precipitates was replaced with ethanol (the sample was designated as nano-GZh-2). The procedure developed for the synthesis allowed us to reproducibly form nanodisperse Fe^{3+} hydroxides, to minimize the interaction between nanoparticles in the gel structure, and to prevent their crystallization and growth at the stage of sample preparation. The nano-GZh-1 and nano-GZh-2 samples, which were washed to remove impurities and dried in a dry oven at 60°C for 16 h, are considered below as initial samples.

Adsorption measurements. The samples were characterized by the low-temperature (77 K) sorption of nitrogen and molecular hydrogen using a DigiSorb-2600 Micromeritics instrument. Before adsorption measurements, the samples were heat-treated in vacuo at a residual pressure of 10^{-3} Torr and varied temperature over different periods of time. Tables 1 and 2 summarize the measured texture parameters of nanodisperse hydroxide samples, where $\gamma = (m_{init} - m_{fin})/m_{init}$ (g/g) is the change in the sample weight in the course of thermal vacuum treatment; S_{BET} is the BET surface area; $S_\alpha^{N_2}$ is the mesopore surface area and $V_\mu^{N_2}$ is the micropore volume derived from nitrogen sorption isotherms by the comparative method [18]; V_s is the limiting volume of the sorption space, including the micropore and mesopore volumes; $V_\mu^{H_2}$ is the micropore volume calculated from hydrogen sorption isotherms by the comparative volumetric method [19]; and S_{out} is the surface area of primary particle aggregates determined by the comparative method from the $(0.90–0.97)P/P_0$ portion of the nitrogen desorption isotherm [20]. The mesopore size distribution was calcu-

Table 2. Texture characteristics of the nano-GZh-2 samples

Sample no.	Thermal treatment conditions, °C/time, h	γ	C_{BET}	$S_{\alpha}^{N_2}$, m^2/g	$V_{\mu}^{N_2}$, cm^3/g	$V_{\mu}^{H_2}$, cm^3/g
1	Vacuum 150/5	0.177	–1100	112	0.020	0.020
2	Vacuum 150/12	0.137	–14500	130	0.022	0.022 (+1 cm^3 (STP)/g)
3	Vacuum 150/24	0.170	800	145	0.021	0.022 (+1.6 cm^3 (STP)/g)
4	Vacuum 150/36	0.173	213	147	0.020	0.023 (+1.7 cm^3 (STP)/g)

lated from the desorption branch of nitrogen sorption isotherms using the classical Barrett–Joiner–Halenda (BJH) method [21].

Electron microscopic studies. The size, morphology, and substructure of synthesized nanodisperse iron hydroxide particles; the particle size distribution; and the particle packing in dry hydrogels (xerogels) were studied by transmission electron microscopy (TEM) on a JEM-2010FX high-resolution electron microscope (accelerating voltage, 200 kV; resolution, 1.4 Å) with the use of standard sample preparation procedures.

X-ray diffraction. The X-ray diffraction analysis of samples was performed on a Siemens D-500 diffractometer using the point-by-point scan technique ($2\Theta = 10°–70°$, 0.05° increments, accumulation time of 5 s).

Thermogravimetric analysis. The complex thermogravimetric analysis of nanosized iron hydroxides was performed on a Netzsch STA 449C thermoanalytical system at a heating rate of 2 K/min with the use of 200-mg samples.

RESULTS AND DISCUSSION

The procedure developed for the synthesis resulted in the formation of nanodisperse Fe^{3+} hydroxides and prevented the crystallization and growth of particles at the stages of synthesis and sample preparation. Indeed, we found using electron microscopy that the nano-GZh-1 sample in the initial state consisted of approximately spherical particles with a narrow particle-size distribution ($d = 2.5–3.5$ nm), which were aggregated in the pore structure of iron xerogels (Fig. 1a). After the thermal treatment of the nano-GZh-1 sample in air at 150°C for 130 h (Fig. 1b), it mainly consisted of particles with a size of ~3 nm as before. At the same time, elongated particles with sizes of $\sim 9 \times 3$ nm appeared in the sample; this fact suggests the possibility of oriented interactions between two or three smaller particles under the specified sample heating conditions. The nano-GZh-2 sample also mainly consisted of particles 2.5–3.5 nm in diameter. The occurrence of regions with pronounced signs of changes in the morphology of aggregates was surprising. This manifested itself in the self-organization of nanosized particles into two-dimensional layers packed in multilayered units. It is believed that the replacement of water by ethanol in Fe^{3+} hydroxide hydrogel at the stage of sample washing to remove impurity salts facilitates the appearance of the self-organization effect of nanodisperse particles. A small amount of unremovable NH_4NO_3 salt was also detected in the nano-GZh-2 sample (Fig. 2).

The formation of nanodisperse particles of iron hydroxides from the key polynuclear hydroxo complexes of Fe^{3+}, which was found previously [12–14], allowed us to hypothesize that these particles can have

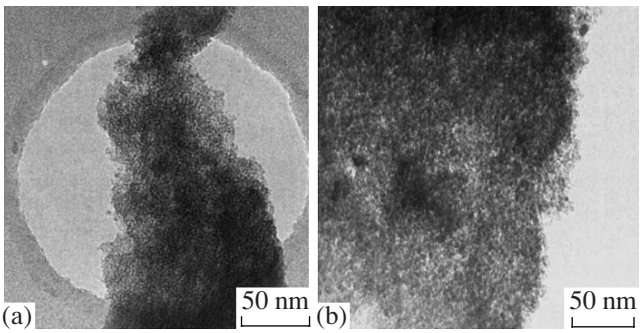

Fig. 1. Electron micrographs of the nano-GZh-1 sample (a) in the initial state and (b) after heating at 150°C in a drying oven for 130 h.

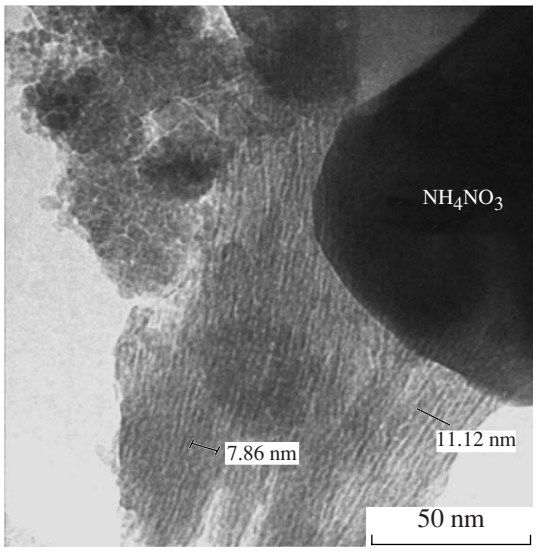

Fig. 2. Electron micrograph of the nano-GZh-2 sample in the initial state.

an internal substructure. To test experimentally the formulated hypothesis, we used light-field and dark-field TEM techniques, which allowed us to detect local ordering regions in nanodisperse Fe^{3+} hydroxides and to determine their sizes. The theory of the formation of light-field and dark-field images in electron microscopy was considered by Hirsch et al. [22]. In the studies, the samples of nanodisperse Fe^{3+} hydroxides were supported as ethanol suspensions onto carbon substrates with holes. The electron microdiffraction images of these samples exhibited diffuse rings with the averaged interplanar spacings d/n = 2.6 (s), 2.27 (m), and 1.50 Å (w) (not given). The sizes of coherent-scattering regions calculated from the broadenings of diffraction rings were 3–5 nm.

According to the X-ray diffraction data for the nano-GZh-1 sample in the initial state, two diffuse peaks at interplanar spacings d of ~2.61 and ~1.51 Å can be recognized, which cannot be reliably attributed to particular known modifications of iron hydroxides or oxides. The X-ray diffraction pattern of the nano-GZh-2 sample was similar to that of nano-GZh-1. The calculations of coherent-scattering regions from the halfwidths of these peaks using the well-known Selyakov–Scherrer equation afforded values of 3–5 nm, which are consistent with electron diffraction data.

For dark-field studies, regions of the most intense diffraction rings corresponding to the average d/n = 2.6 Å were separated by an aperture diaphragm. A dark-field image of nanodisperse Fe^{3+} hydroxide is a gray uncontrasted background, against which pronounced well-defined spots no more than 1.0 nm in size can be seen. A comparison between light-field and dark-field images suggests that the spots have a diffraction rather than absorption character. In other words, the spots are due to the occurrence of structurally ordered regions with sizes of ~1 nm in the bulk of the nanoparticles. As the hole diameters in aperture diaphragms were increased from 20 to 120 μm, spot sizes in dark-field images remained unchanged; only the concentration of spots increased. This fact suggests that the sizes and the nature of ordering of the regions were the same. The spatial separation of dark-field images suggests the occurrence of disorientation between ordered regions in the bulk of nanoparticles. As estimated according to Hirsch et al. [22] with the use of our data, disorientation angles can be as large as a few degrees.

Figure 3 shows the results of complex thermogravimetric analysis of the initial nano-GZh-1 sample and the sample dried in air at 150°C. In accordance with the interpretation of effects in the thermograms of highly dispersed Fe^{3+} hydroxides, which was given by Krivoruchko et al. [12], the effect of weight loss with an extremum temperature of 157°C on heating the initial sample under nonisothermal conditions (Fig. 3a) was due to the removal of adsorbed and coordinatively bound water and a shoulder at 207°C was due to the loss of the reaction products of basic OH groups with acid protons of bridging OH groups. Effects at 279, 316, and 364°C were due to the removal of OH groups with different bonding energies from the bulk of nanoparticles. Note that the weight loss effect at 316°C was associated with an exothermal effect of the crystallization of oxide nanoparticles with the formation of coarsely dispersed α-Fe_2O_3 crystals. In the thermogram of the nano-GZh-1 sample dried at 150°C (Fig. 3b), effects at 157 and 207°C shifted by ~30°C to the low-temperature region. The other thermal effects did not change their positions on the temperature scale.

From data in Fig. 3a, it follows that the composition of nano-GZh-1 is expressed by the approximate empirical formula $Fe_2O_3 \cdot 1.8H_2O$. In the initial nano-GZh-1 sample, the coordination number of Fe^{3+} cations with respect to oxygen was close to 6 [12, 14]. In the general case, these cations contain crystal water, OH^-, and O^{2-} in the first coordination sphere. In the thermogram of the nano-GZh-2 sample, the number and positions of thermal effects were almost identical to those shown in Fig. 3a.

According to thermogravimetric analysis data, the thermograms of the nano-GZh-1 and nano-GZh-2 samples exhibited endothermic effects over the range of 60–270°C due to the dehydration of Fe^{3+} hydroxides and an exothermic effect at 280–360°C (a maximum temperature of 322°C) due to the crystallization of oxide nanoparticles. Based on these results, we chose conditions for the thermal treatment of iron hydroxides to obtain nanodisperse xerogels for texture studies.

The micropore structure of the nano-GZh-1 and nano-GZh-2 samples was studied by the molecular probe method with the use of the low-temperature (77 K) adsorption of nitrogen and molecular hydrogen (the kinetic sizes of N_2 and H_2 molecules are σ_k = 0.364 and 0.289 nm, respectively [23]).

The adsorption isotherms of nitrogen vapor at 77 K for the nano-GZh-1 and nano-GZh-2 samples (Figs. 4, 5) exhibited a weakly pronounced capillary condensation hysteresis, which suggests that the predominant characteristic pore size in these materials is smaller than 3 nm. After the thermal treatment of these samples in air at 150°C for 130 h, the adsorption isotherms of nitrogen exhibited a hysteresis in the region of $0.4 < P/P_0 < 0.7$. This also suggests the occurrence of only small mesopores (smaller than 5 nm).

From data given in Table 1, it follows that the micropore volume cannot be determined in all of the samples subjected to thermal vacuum treatment using traditional methods for the analysis of nitrogen adsorption isotherms on the nano-GZh-1 sample; in particular, this manifested itself in underestimated values of the energy constant of the BET equation (C_{BET}). It is well known [18, 24] that the presence of micropores in the samples resulted in C_{BET} higher than the characteristic value of 100. Then, as the micropore volume increased, the formally calculated values of C_{BET} as a function of

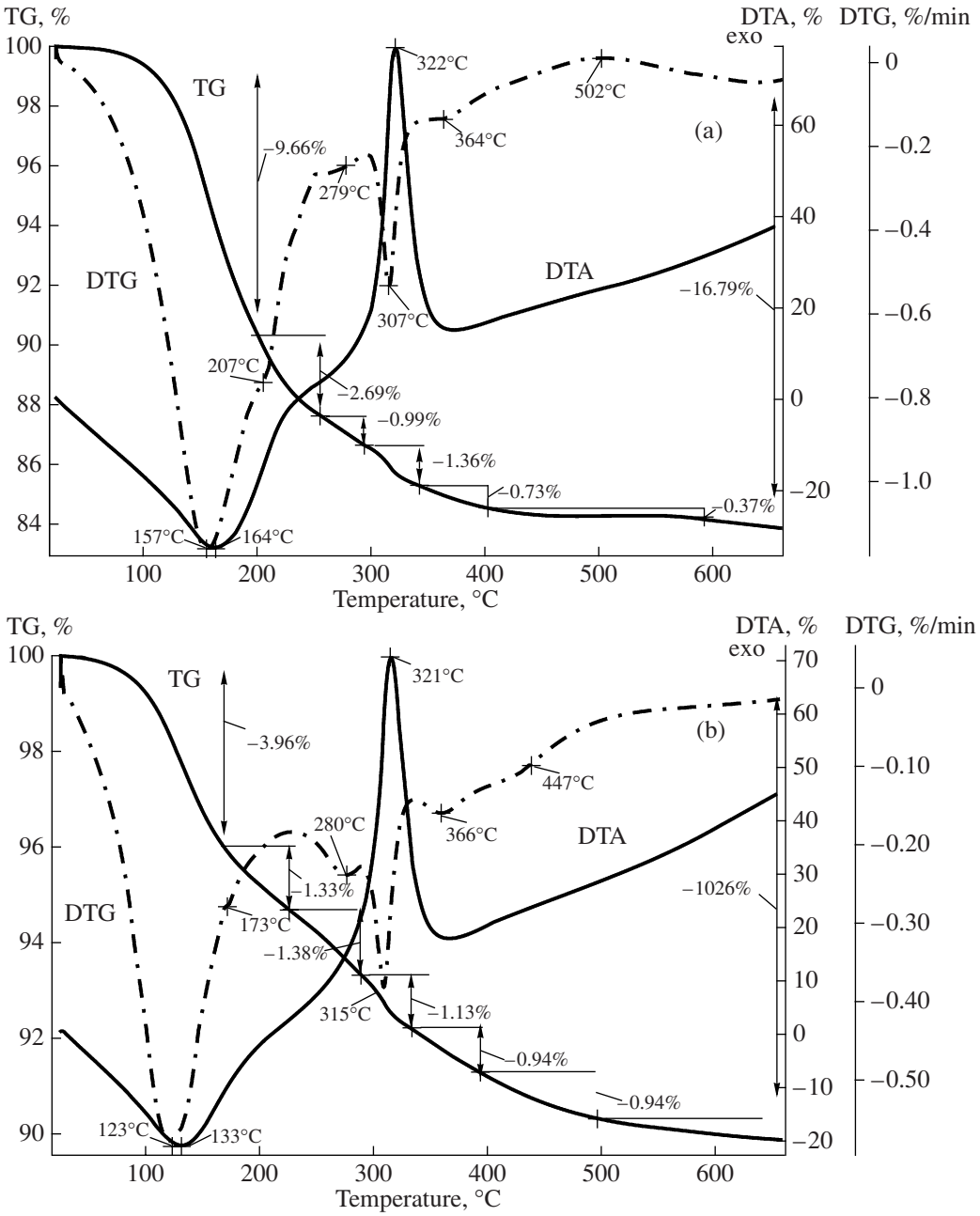

Fig. 3. Thermoanalytical curves for (a) the initial nano-GZh-1 sample and (b) the nano-GZh-1 sample after heating at 150°C in a drying oven for 130 h.

micropore volume underwent a discontinuity and changed to the region of negative values. This change in the energy constant C_{BET} occurred in the nano-GZh-2 samples (Table 2); this fact is indicative of a developed micropore structure in these samples. Correspondingly, traditional comparative analysis of nitrogen adsorption isotherms [18] did not allow us to obtain reliable data on the micropore structure of the nano-GZh-1 samples.

The specific interaction of nitrogen molecules with the nano-GZh-1 and nano-GZh-2 samples supported the above properties of surface layers in highly dispersed samples according to electron-microscopic data. In the former case (nano-GZh-1), thin-walled structures were produced, which formed multilayered formations (nano-GZh-2) under synthesis conditions that facilitated the self-organization of particles. These properties of the samples explain the weakened intermolecular interaction of the sorbate with a thin wall of nano-GZh-1 and the strong interaction for the more multilayered structure of nano-GZh-2. For model systems (mixed samples of ZSM-5 zeolite and highly dis-

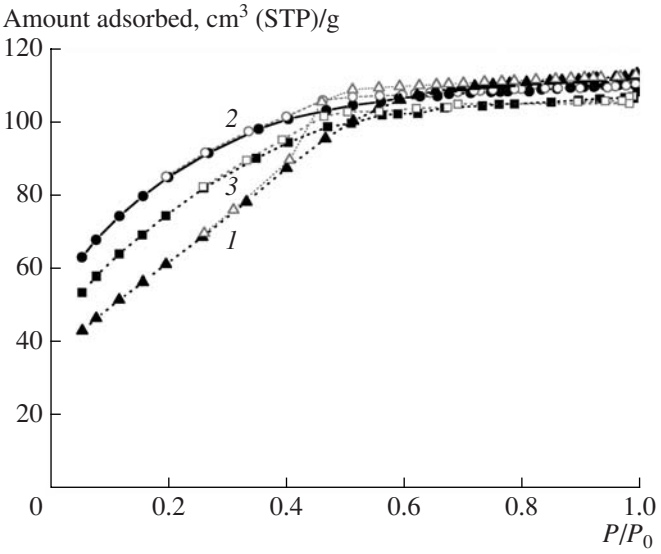

Fig. 4. Isotherms of N_2 sorption (77 K) on the nano-GZh-1 samples (see Table 1): (*1*) sample no. 2, (*2*) sample no. 3, and (*3*) sample no. 6.

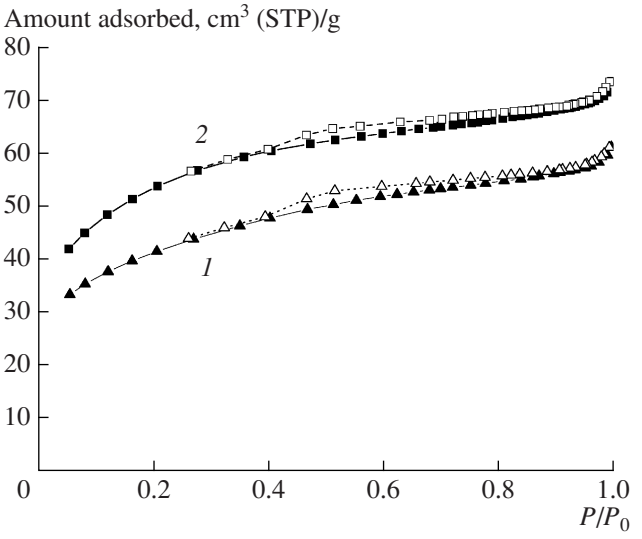

Fig. 5. Isotherms of N_2 sorption (77 K) on the nano-GZh-2 samples (see Table 2): (*1*) sample no. 1 and (*2*) sample no. 4.

persed MCM-41 silicate material), the sorption of nitrogen of this kind was considered in detail elsewhere [24].

To study meso- and microporous systems that combine regions with an increased sorption potential and regions with weak sorption interactions with nitrogen molecules, the sorption of molecular hydrogen can be used [25]. Figure 6 exemplifies the sorption isotherms of molecular hydrogen on the nano-GZh-1 test samples. It can be seen that the adsorption–desorption isotherms are reversible; this fact suggests the process occurs under the action of dispersion intermolecular interactions. The procedure developed for the comparative adsorption analysis [25, 26] makes it possible to determine the micropore volume $V_\mu^{H_2}$ in the nano-GZh-1 samples (Table 1). This behavior of nitrogen and hydrogen sorbates suggests a highly dispersed state of the nano-GZh-1 sample and the possible formation of micropores both in the bulk of nanoparticles and in the interlayer structure of nanoparticle packing.

The set of experimental data given in Table 1 allowed us to distinguish a number of factors in the texture changes of Fe^{3+} nanohydroxides. In general, an increase in the treatment temperature (an increase in the degree of dehydration) facilitated a decrease in the micropore volume $V_\mu^{H_2}$, the specific surface area of mesopores $S_\alpha^{N_2}$, and the total micropore volume V_s. However, the intensity of changes in these parameters essentially depended on the thermal treatment procedure, as can be seen clearly in Fig. 7. The intensity of texture changes reached a maximum upon the treatment of the samples in air in a drying oven. At the same time, the aggregation of primary hydroxide nanoparticles, which can be evaluated from the outer surface area of aggregates S_{out} and the related aggregate size, did not correlate with the dehydration procedure. According to approximate evaluations, the sizes of these aggregates were constant to a first approximation and amounted to about 700–1000 nm. The structure of aggregates was characterized by a sufficiently high packing density of particles with a porosity of 0.35–0.37, based on the density of chemically similar iron hydroxide of 3.5 g/cm^3 [14] and the total pore volume of 0.18–0.17 cm^3/g of the samples.

Note that an increase in the time of thermal vacuum treatment at 150°C from 5 to 24 h did not cause considerable changes in the hydroxide texture parameters

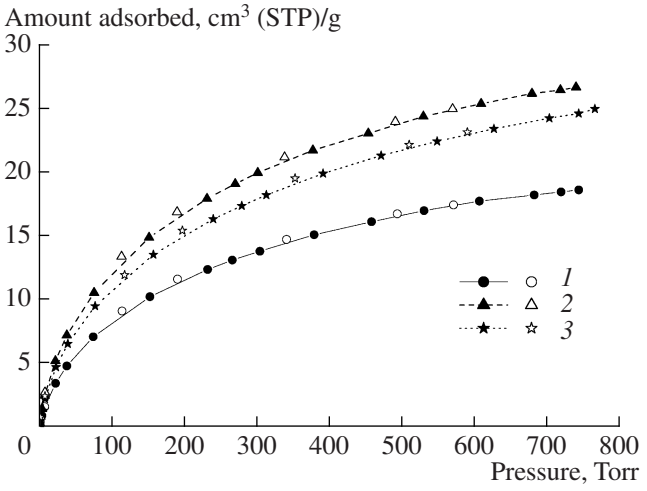

Fig. 6. Isotherms of H_2 sorption–desorption (77 K) on the nano-GZh-1 samples (see Table 1): (*1*) sample no. 2, (*2*) sample no. 3, and (*3*) sample no. 6.

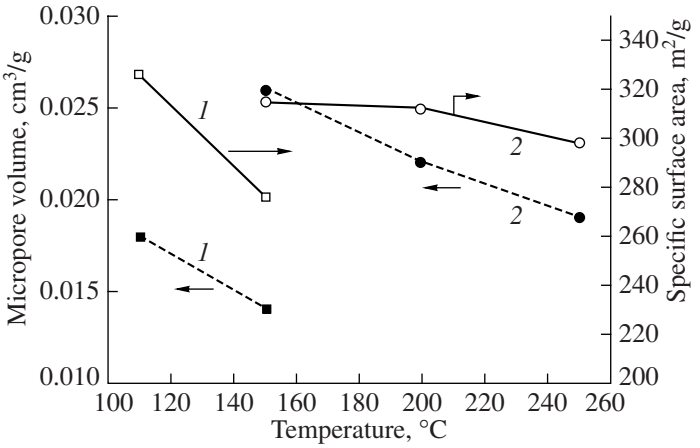

Fig. 7. Changes in the micropore volume and specific surface area of mesopores in the nano-GZh-1 samples upon thermal treatment (*1*) in air in a drying oven and (*2*) in a vacuum.

(S_α and V_μ) with a simultaneous decrease in the value of V_s, although considerable dehydration of the samples occurred under these conditions, as follows from the change in the value of γ. Based on the above empirical formula of iron hydroxides, vacuum dehydration at 250°C resulted in the removal of more than 80% of the initial amount of structure water.

As can be seen in Table 1, changes in the mesopore structure suggest that the volume of the thinnest mesopores with $d < 3$ nm decreased under mild thermal vacuum treatment conditions (150–250°C). Simultaneously, a detectable amount of mesopores with sizes of 3.4–3.6 nm appeared at 250°C (Fig. 8) with a simultaneous decrease in the total mesopore and micropore volume (V_s). In the samples treated in air in a drying oven, pores with the above size were formed at a lower temperature (110°C), whereas the volume of these pores was considerable at 150°C. Note that mesopores with a characteristic size of 3.5 nm were also formed in the dehydration of the nano-GZh-2 sample. It is believed that the appearance of a detectable volume of pores with a characteristic size of 3.5 nm was associated with the formation of particles with close sizes in the course of dehydration regardless of dehydration procedure. In general, this supports the above electron-microscopic data. A rearrangement of the mesopore texture of the samples with a total decrease in the pore volume suggests the mutual mobility of nanoparticles on a nanoaggregate level; this mobility was retained up to high degrees of dehydration. Consequently, the removal of crystal water did not result in the formation of strong chemical bonds between particles and comparatively weak coagulation bonds with weak interaction energies were responsible for the aggregation of nanoparticles.

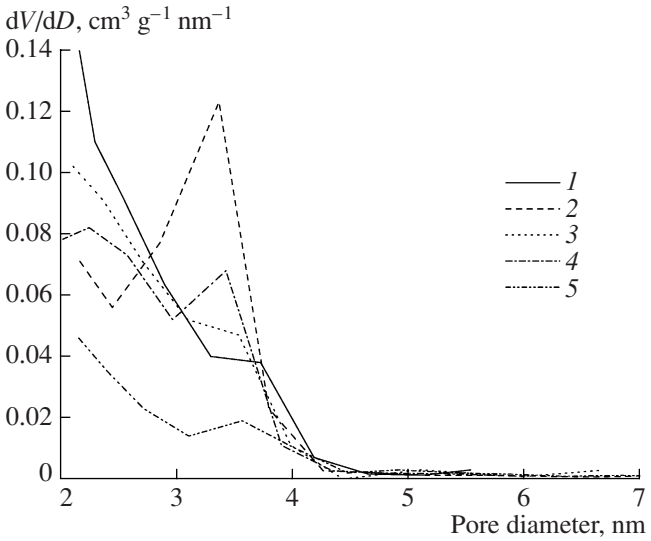

Fig. 8. Mesopore-size distribution for the nano-GZh-1 and nano-GZh-2 samples after various thermal treatments (see Table 1): (*1*) sample no. 3, (*2*) sample no. 2, (*3*) sample no. 6, (*4*) sample no. 7, and (*5*) sample no. 4 (Table 2).

Data in Table 2 indicate that the microtexture (V_μ) of the nano-GZh-2 samples remained almost unchanged under the specified conditions of dehydration. In addition, an increase in the surface area S_α suggests an increase in the volumes of the thinnest pores. Differential mesopore-size distribution curves are indicative of an increase in the volumes of mesopores with a size of 3–3.5 nm. Note that the volumes of micropores V_μ accessible to nitrogen and hydrogen molecules in the nano-GZh-2 test samples of xerogels coincided.

It is believed that the micropore volume V_μ, which appeared at a minimum degree of dehydration and remained unchanged with increasing γ, corresponds to the appearance of an internal substructure of nanoparticles.

At the same time, the nano-GZh-2 samples subjected to thermal vacuum treatment for 12, 24, and 36 h (Table 2) exhibited insignificant values of the specific sorption of H_2 (~1, 1.6, and 1.7 cm^3(STP)/g, respec-

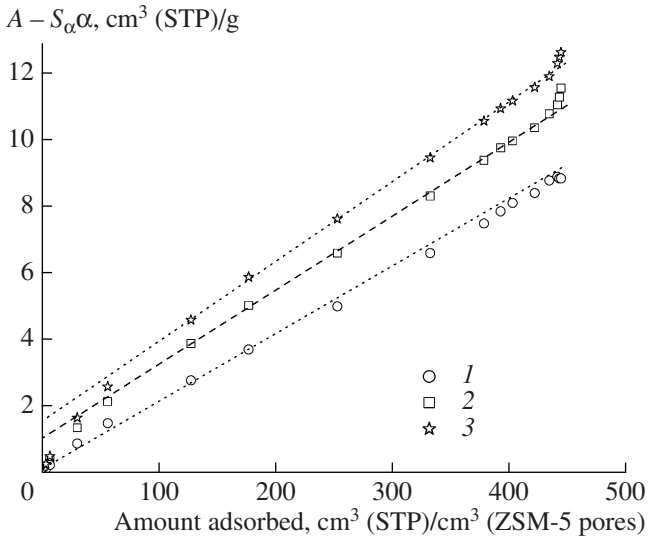

Fig. 9. Processing of H_2 sorption isotherms (77 K) by the comparative volumetric method for the nano-GZh-2 samples (see Table 2): (*1*) sample no. 1; (*2*) sample no. 2, and (*3*) sample no. 3.

tively; intercepts in the axis of ordinates in the comparative plots shown in Fig. 9 [19]). They can be interpreted as sorption in the thinnest ultramicropores accessible only to hydrogen molecules. It is believed that these ultramicropores were formed in the course of long thermal vacuum dehydration in the interlayer space of the self-organized nanodisperse particles of iron oxide.

CONCLUSIONS

Thus, we developed a preparation procedure and synthesized the samples of nanodisperse iron hydroxide with a narrow particle-size distribution (2.5–3.5 nm). We were the first to detect a substructure in the bulk of the nanoparticles of Fe^{3+} hydroxide. We found that structurally ordered regions with sizes of ~1.0 nm disoriented with respect to each other at angles of a few degrees occurred in the bulk of nanoparticles. We demonstrated that, in principle, self-organized layered structures of iron nanohydroxide (oxide) can be produced.

The synthesized nanodisperse iron hydroxide had the empirical formula ~$Fe_2O_3 \cdot 1.8H_2O$ and contained crystal water, OH groups, and Fe^{3+} cations in an octahedral oxygen coordination. We found that structural and nonstructural water can be removed almost completely from the bulk of nanoparticles over the temperature range of 150–250°C with the retention of an X-ray amorphous character and visually observable sizes. Moreover, mesopores with diameters d of ~3.5 nm were progressively formed in iron oxide xerogels in the course of dehydration with a simultaneous decrease in the total pore volume. This suggests a retained mutual mobility of particles and weak bond energies of particles in aggregates. In addition, a detectable volume of micropores was formed in the structure. In the nano-GZh-2 sample, which contained the regions of self-organized layered structures of initial nanoparticles, an insignificant volume of ultramicropores accessible only to hydrogen molecules was additionally formed.

ACKNOWLEDGMENTS

We are grateful to V.I. Zaikovskii for the electron micrographs and to G.S. Litvak for the thermogravimetric analysis of nanodisperse iron hydroxide samples.

This work was supported by the Russian Foundation for Basic Research (project no. 06-03-33107).

REFERENCES

1. Molchanov, V.V., Andrushkevich, M.M., Plyasova, L.M., Buyanov, R.A., and Kotel'nikov, G.R., *Kinet. Katal.*, 1988, vol. 29, no. 1, p. 248.
2. Kotel'nikov, G.R. and Bespalov, V.P., *Katal. Prom–sti.*, 2002, no. 4, p. 10.
3. Oliveira, A.C.V., Fierro J.L.G., Valentini, A., Nobre, P.S.S., and Rangel, M.C., *Catal. Today*, 2003, vol. 85, no. 1, p. 49.
4. Arata, K., Matsuhashi, H., Hino, M., and Nakamura, H., *Catal. Today*, 2003, vol. 81, no. 1, p. 17.
5. Daniells, S.T., Overweg, A.R., Makkee, M., and Moulijn, J.A., *J. Catal.*, 2005, vol. 230, no. 1, p. 52.
6. Buyanov, R.A., Krivoruchko, O.P., Kefeli, L.M., and Ostan'kovich, A.A., *Kinet. Katal.*, 1968, vol. 9, no. 2, p. 379.
7. Buyanov, R.A., Krivoruchko, O.P., and Golovin, A.V., *Kinet. Katal.*, 1968, vol. 9, no. 4, p. 804.
8. US Patent No. 5047382, 1991.
9. Li, P., Miser, D.E., Rabiei, S., Yadav, R.T., and Hajaligol, M.R., *Appl. Catal., B*, 2003, vol. 43, no. 2, p. 151.
10. Taghiei, M.M., Huggins, F.E., Ganguly, B., and Huffman, G.P., *Energy Fuels*, 1993, vol. 7, no. 3, p. 399.
11. Huffman, G.P., Ganguly, B., Zhao, J., Rao, K.R.P.M., Shah, N., Feng, Z., Huggins, F.E., Taghiei, M.M., Lu, F., Wender, I., Pradhan, V.R., Tierney, J.W., Seehra, M.M., Ibrahim, M.M., Shabtai, J., and Eyring, E.M., *Energy Fuels*, 1993, vol. 7, no. 2, p. 285.
12. Krivoruchko, O.P., Buyanov, R.A., Zolotovskii, B.P., and Ostan'kovich, A.A., *Izv. Akad. Nauk SSSR, Ser. Khim.*, 1974, no. 7, p. 1460.
13. Fedotov, M.A., Krivoruchko, O.P., Buyanov, R.A., and Zolotovskii, B.P., *Izv. Akad. Nauk SSSR, Ser. Khim.*, 1975, no. 8, p. 1705.
14. Kriger, T.A., Krivoruchko, O.P., and Buyanov, R.A., *React. Kinet. Catal. Lett.*, 1984, vol. 24, nos. 3–4, p. 401.
15. Buyanov, R.A. and Krivoruchko, O.P., *Kinet. Katal.*, 1976, vol. 17, no. 3, p. 765.
16. Malakhov, V.V., Krivoruchko, O.P., Lokotko, L.F., Trukhacheva, V.A., and Buyanov, R.A., *Kinet. Katal.*, 1978, vol. 19, no. 2, p. 447.

17. Krivoruchko, O.P., Malakhov, V.V., and Ermakova, A., Buyanov, R.A., and Lokotko, L.F., *Kinet. Katal.*, 1987, vol. 28, no. 2, p. 442.
18. Karnaukhov, A.P., *Adsorbtsiya: Tekstura dispersnykh i poristykh materialov* (Adsorption: Texture of Disperse and Porous Materials), Novosibirsk: Nauka, 1999.
19. Gavrilov, V.Yu., *Kinet. Katal.*, 1995, vol. 36, no. 5, p. 787.
20. Gavrilov, V.Yu., Fenelonov, V.B., Zheivot, V.I., and Shalaeva, M.E., *Kinet. Katal.*, 1987, vol. 28, no. 4, p. 959.
21. Gregg, S.J. and Sing, K.S.W., *Adsorption, Surface Area, and Porosity*, London: Academic, 1967.
22. Hirsch, P., Howie, A., Nicholson, R., Pashley, D., and Whelan, M., *Electron Microscopy of Thin Crystals*, London: Butterworths, 1965.
23. Breck, D., *Zeolite Molecular Sieves: Structure, Chemistry and Use*, New York: Wiley, 1974.
24. Gavrilov, V.Yu. and Sokolov, E.E., *Kinet. Katal.*, 2007, vol. 48, no. 6, p. 851 [*Kinet. Catal.* (Engl. Transl.), vol. 48, no. 6, p. 794].
25. Gavrilov, V.Yu., *Kinet. Katal.*, 2007, vol. 48, no. 6, p. 856 [*Kinet. Catal.* (Engl. Transl.), vol. 48, no. 6, p. 799].
26. Gavrilov, V.Yu., *Kinet. Katal.*, 2005, vol. 46, no. 4, p. 642 [*Kinet. Catal.* (Engl. Transl.), vol. 46, no. 4, p. 603].